Advance Controller for Power Quality and Performance Improvement of Grid-Connected Single-Phase Rooftop PVS

Jitendra Kumar Singh, *Member, IEEE*, Khaled Al Jaafari, *Senior Member, IEEE*, Hatem H. Zeineldin, *Senior Member, IEEE*, Ranjan Kumar Behera, *Senior Member, IEEE*, Ahmed Al-Durra, *Senior Member, IEEE*, and Ehab El-Saadany, *Fellow, IEEE*

***Abstract*— This article presents a robust controller for a single-phase single-stage photovoltaic systems (PVSs) converter connected to the grid. A high-efficiency single-phase single-stage converters are prone to double-frequency oscillations and dc-link voltage fluctuations when connected to a PVS. It introduces phase shift and injects harmonics in the grid current. To address this issue, a robust dc-link voltage controller is proposed. It can achieve a fast transient response with lesser overshoot under power intermittency and grid-side disturbances. A filter is employed to reduce the impact of switching frequency; however, a Lyapunov-based inner loop current controller with an active damping method minimizes the effect of resonance and achieves system stability. The proposed composite controller guarantees the system's robustness against grid disturbances and parameter uncertainties. In addition, it eliminates the effect of phase shift and achieves zero steady-state error. Both the simulation and experimental results are presented to demonstrate the performance of the controller.**

***Index Terms*— Current control, dc-link control, double-frequency ripple, nonlinear controller, power conversion harmonics, power quality, renewable integration.**

Manuscript received 22 May 2023; revised 19 September 2023 and 6 March 2024; accepted 12 April 2024. Date of publication 22 April 2024; date of current version 4 June 2024. This work was supported by ASPIRE, the Technology Program Management Pillar of Abu Dhabi's Advanced Technology Research Council (ATRC), via the ASPIRE "Virtual Research Institute (VRI) Award"; and in part by the research grant by "NIDHI-PRAYAS Scheme of NSTEDB," DST, Incubation Centre IIT Patna. Recommended for publication by Associate Editor Marta Molinas. *(Corresponding author: Jitendra Kumar Singh.)*

Jitendra Kumar Singh, Khaled Al Jaafari, Ahmed Al-Durra, and Ehab El-Saadany are with the Advanced Power and Energy Center (APEC), Department of Electrical Engineering, Khalifa University, Abu Dhabi, United Arab Emirates (e-mail: jitendra1603@gmail.com; khaled.aljaafari@ku.ac.ae; ahmed.aldurra@ku.ac.ae; ehab.elsadaany@ku.ac.ae).

Hatem H. Zeineldin is with the Advanced Power and Energy Center (APEC), Department of Electrical Engineering, Khalifa University, Abu Dhabi, United Arab Emirates, and also with the Electric Power Engineering Department, Cairo University, Giza 12613, Egypt (e-mail: hatem.zeineldin@ku.ac.ae).

Ranjan Kumar Behera is with the Department of Electrical Engineering, Indian Institute of Technology Patna, Bihta 801103, India.

Color versions of one or more figures in this article are available at https://doi.org/10.1109/JESTPE.2024.3392245.

Digital Object Identifier 10.1109/JESTPE.2024.3392245

NOMENCLATURE

S_u, Δs_u	Switching states in steady-state and perturb state.
$V_{\rm dc}$, V_c	DC-link voltage and capacitor voltage.
$V_{\rm dcref}$	Reference dc-link voltage.
I_i, I_g	Inverter current and grid current.
L_i, L_g	Inverter- and grid-side inductances.
C, $C_{\rm dc}$	Filter capacitance and dc-link capacitance.
r_i, r_g	Inverter- and grid-side internal resistances.
k_p, k_i	Proportional and integral constant of PI.
K_p, K_r	Proportional and resonant constant of PR.
ω, ω_c	Natural frequency and cutoff frequency.

I. INTRODUCTION

IN DISTRIBUTED generation (DG) systems, the advancement of renewable energy sources increases the role of small-scale photovoltaic (PV) integrated systems [1]. These systems mainly focused on increasing efficiency, reliability, power density, and cost reduction [2]. To achieve this, various converter topologies are discussed to improve the power density at a lesser cost [2], [3]. Typically, more than one conversion stage reduces the power density and reliability of the system. Therefore, in grid-connected PV (GCPV) systems, single-stage power converters are convenient to achieve high efficacy and reliability. However, in single-stage GCPV systems, due to single-stage conversion, a rapid change in dc-link voltage dynamics may lead to stability issues.

The increased integration of PV-based systems as DG raises the concern of system dynamics and stability during grid disturbances, such as voltage sag and load change. To achieve the desired stability level, a fast dynamic response controller is inevitable. The dynamic analysis of such systems can be classified as the dynamic response of the dc-link voltage controller (typically in the range of 0.1 s) and the dynamic response of the current controller (typically within 0.01 s) [4], [5]. Therefore, various control methodologies are adopted to improve the system's performance. This can be normally achieved by the development of a robust outer loop control for voltage regulation [6] and integration of an all-pass filter in the current

controller [7]. In a single-stage system, the GCPV system has to perform all operations related to the stable dc-link voltage, maximum power extraction from the PV source, and grid current reference generation. However, the major concerns of the single-stage GCPV system are the high power quality and stability. Moreover, the utilization of the LCL filter introduces additional poles, which causes a resonance issue and further influences the stability of the system [8]. Therefore, a current controller with active damping is usually employed [9]. This increases the requirement for a robust controller to address the PV- and grid-side disturbances.

Recently, nonlinear controllers have been proposed to improve the performance and suppress the disturbances [10]. These nonlinear controllers enhance the system dynamics and achieve a large stability margin [11], [12], [13], [14]. However, the feedback linearization approach discussed in [12] and [13] has low-power quality. In [14], an H_∞ controller is discussed for dc-link voltage regulation and μ synthesis current controller for grid-side control. It can achieve robustness against grid impedance variation with lesser number of sensors and compensates for the time delay. The focus is to improve both the transient response and disturbance rejection capability. However, it operates at a high switching frequency and has high dc-link voltage ripple and overshoot with higher controller complexity. An adaptive gain observer is used in [15] to achieve good disturbance rejection and reduce the sensitivity to noise. However, the inclusion of the nonlinear controller causes variable switching frequency and has a steady-state error in the grid current [10], [15]. In [16], an active disturbance rejection controller (ADRC) is discussed to regulate the dc-link voltage of the GCPV system, which is imminent for power quality improvement. However, this method is discussed only for three-phase systems and has high complexity. In single-phase GCPV systems, the double-frequency oscillation across dc-link voltage increases the harmonics injected into the grid current and reduces the power quality of the system. Moreover, in a single-stage single-phase GCPV system, dc-link voltage fluctuation and phase shift are introduced due to the input PV power intermittency and double line frequency, respectively. Furthermore, during grid-side disturbances such as voltage sag and load change, these oscillations become more severe, which requires a fast transient response for achieving system stability. Moreover, the impact of dynamic and server load change is not discussed at the DG level. The voltage deviation across dc-link from its nominal value may damage the inverter switches or dc-link capacitor, which can further initiate the protection devices and cause an involuntary shutdown of the GCPV system [17].

To address the issues related to single-phase single-stage systems, various nonlinear current controllers and adaptive PI approaches for dc-link voltage control are discussed in [18], [19], and [20]. In [18], a nonlinear PI (NPI) approach is utilized to reduce the harmonic content by scheduling the gain to the change in the error signal. However, with changes in the error signal, recalculation of the gain is required, which introduces a processing delay and necessitates advanced processors. An NPI predictive controller is proposed in [19] for a two-stage three-phase GCPV system, which gives high tracking performance. However, the utilization of the model predictive approach increases the complexity. Moreover, the grid voltage is considered balanced; thus, system uncertainties (such as inductance variation) and grid-side disturbances are not considered. An adaptive PI controller for dc-link voltage control of a single-phase grid-connected ac/dc converter is discussed in [20]. It addresses the double-frequency oscillation issue and dc-link voltage fluctuation, considering a resistive load at dc-link. However, it has a slow dynamic response, high operating switching frequency, and limited grid current THD due to the utilization of the L filter. To reduce the effect of double-frequency ripple in the reference current generation, a notch filter-based approach is utilized in [21] and [22]. However, it affects the transient response of the system. Moreover, an effective active decoupling method is discussed in [23] to eliminate the double-frequency ripple, which requires additional hardware for the circuit. In [24], a moving average filter (MAF) is utilized in the reference current generation loop to reduce the low-frequency current ripple. However, the utilization of the linear controller limits the dynamic performance and disturbance rejection capability. Furthermore, in a single-phase GCPV system, the perturbation and system parameter variation adversely affect the performance of the current feeding into the grid and dc-link voltage, which can jeopardize the stability under load change and grid disturbances [25], [26].

Therefore, to achieve stability in cohesion with fast transient response, an NPI controller in conjunction with the Lyapunov-based inner loop controller is proposed in this article. Moreover, an MAF is employed in the current reference generation loop to eliminate the effect of double-frequency ripples and reduce the grid current harmonics. The NPI controller in the outer loop can provide a fast transient response and good disturbance rejection by adaptively adjusting the gain based on the input error signal. Thus, it renders a high gain when the dc-link error is small and a low gain when the error is high. The proposed NPI controller counteracts the delay introduced by the MAF in the current loop and achieves unity power factor (upf) operation. Moreover, the proposed control loop introduces a switching function to eliminate phase delay and limit noise sensitivity. Furthermore, the Lyapunov-based inner loop current control helps to attain stability despite internal and external disturbances, as well as parametric uncertainties, and renders active damping by including a capacitor voltage loop. A proportional–resonant (PR) controller is also employed in the inner loop to ascertain the current from the inverter and attains zero steady-state error for the grid current. The proposed controller can address the major issues related to a single-phase single-stage GCPV system. It reduces the effect of the double-frequency oscillation in the reference current generation, thus improving the current quality. Moreover, by achieving upf operation, it eliminates the effect of phase shift caused by loop ripple [17]. Furthermore, it can provide a fast transient response under both PV-side intermittency and grid-side disturbances.

The major contributions of the work are highlighted in the following.

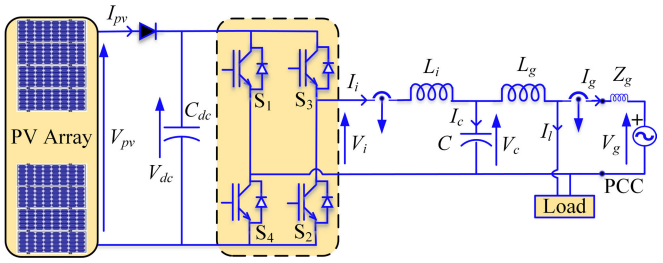

Fig. 1. Single-stage PV integrated grid-connected inverter system with an LCL filter.

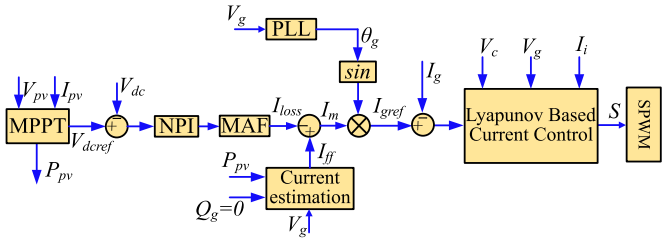

Fig. 2. Proposed control structure for the single-phase single-stage GCPV system.

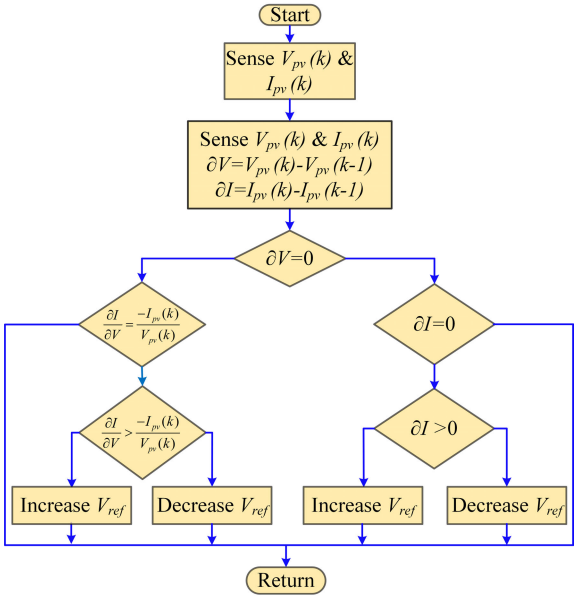

Fig. 3. Flowchart of the incremental conductance MPPT algorithm.

1) An NPI-based outer loop voltage controller is contrived to reduce the dc-link voltage fluctuation and improve the transient response. It can achieve low gain when the error is high and high gain at a smaller value of error.
2) The proposed NPI controller with MAF can effectively reduce the harmonics in the reference grid current, achieving fast tracking of dc-link reference and robustness against system disturbances.
3) A Lyapunov-based inner loop current control can assure the stability of the GCPV system against grid-side uncertainties and reduce the issue of resonance in the grid current.

II. System Modeling

Fig. 1 depicts the schematic of a single-phase PV integrated system connected to the grid with an LCL filter. A stable dc-link voltage can be obtained utilizing a capacitor ($C_{\rm dc}$), connected between the PV array and the voltage-source inverter (VSI) for a single-stage conversion. The operation of the single-stage GCPV system can be described by the state space model in the following equation:

$$L_i\frac{di_i}{dt}=s_u v_i-v_c-r_i i_i,\quad C\frac{dv_c}{dt}=i_i-i_g$$
$$L_g\frac{di_g}{dt}=v_c-v_g-r_g i_g,\quad C_{\rm dc}\frac{dv_{\rm dc}}{dt}=i_{\rm pv}-s_u i_i \tag{1}$$

$$\frac{d}{dt}\begin{bmatrix} i_g\\ i_i\\ v_c\\ v_{\rm dc}\end{bmatrix}=\begin{bmatrix} -\tau_g^{-1} & 0 & L_g^{-1} & 0\\ 0 & -\tau_i^{-1} & -L_i^{-1} & s_u L_i^{-1}\\ -C^{-1} & C^{-1} & 0 & 0\\ 0 & -s_u C_{\rm dc}^{-1} & 0 & 0\end{bmatrix}\begin{bmatrix} i_g\\ i_i\\ v_c\\ v_{\rm dc}\end{bmatrix}+\begin{bmatrix} -L_g^{-1}v_g\\ 0\\ 0\\ r_{\rm pv}^{-1}C_{\rm dc}^{-1}v_{\rm pv}\end{bmatrix} \tag{2}$$

where $\tau_i(=L_i/r_i)$ and $\tau_g(=L_g/r_g)$ represent the inverter- and grid-side inductor time constant, respectively. The inverter output voltage $v_i=s_u.V_{\rm dc}$, and s_u is the switching function of four inverter switches, where u denotes inverter switches $\{1,2,3,4\}$ to control the inverter system. This can be further defined as $s_u=S_u+\Delta s_u$, which includes the switching function in steady-state and perturb deviation of u in the system. The proposed controller utilizing the switching function s_u can further control the state of the system to force the grid current to become sinusoidal and in phase with the grid voltage. The modeling of the system can be described as grid-side current control i_g and PV-side dc-link voltage control $v_{\rm dc}$. Thus, the state variables for grid-side control and PV-side control can be defined by the following equation:

$$x_1=i_i-i_{\rm iref},\quad x_3=v_c-v_{\rm cref}$$
$$x_2=i_g-i_{\rm gref},\quad x_4=v_{\rm dc}-v_{\rm dcref} \tag{3}$$

where i_g, i_i, v_c, and $v_{\rm dc}$ are the measured values of the GCPV system and $i_{\rm gref}$, $i_{\rm iref}$, $v_{\rm cref}$, and $v_{\rm dcref}$ are the estimated references of the proposed controller. In the steady state, assuming that references track the measured values and $s_u=S_u$, the state variable (3) can be applied in the model (1), which simplifies the model as

$$L_i\dot{x}_1=\Delta s_u v_i-x_3-r_i x_1,\quad C\dot{x}_3=x_1-x_2$$
$$L_g\dot{x}_2=x_3-r_g x_2,\quad C_{\rm dc}\dot{x}_4=-x_1 \tag{4}$$

where $\dot{x}$ is the derivative of x.

III. DC-Link Control and Current Quality Improvement

The proposed controller for a single-stage single-phase GCPV system is shown in Fig. 2. To operate a solar array efficiently at its maximum power point (MPP), an incremental conductance-based MPP tracking (MPPT) algorithm is employed, as shown in Fig. 3. It ensures precise and

fast convergence of PV control with minimal computational burden. The MPPT control ensures a consistent dc-link voltage ($v_{\rm dc}^*$) while directing the maximum PV power to the grid [23], [27]. Furthermore, the dc-link voltage regulates the magnitude of grid current, and a maximum power feedforward loop defined by (6) is utilized to improve MPP tracking. The feedforward is crucial to regulate the maximum power from PV to the grid, even in the presence of voltage fluctuations. To improve the dynamic response and reduce the effect of double line frequency, a combination of NPI with MAF control is proposed. The maximum reference grid current can be described as

$$I_m = I_{\rm ff} - I_{\rm loss} \tag{5}$$

$$I_{\rm ff} = \frac{\sqrt{2}P_{\rm pv}}{V_{gm}} \tag{6}$$

where I_m is the magnitude of the maximum reference grid current, $I_{\rm ff}$ is the feedforward current considering no reactive power feeding into the grid for an upf operation, $P_{\rm pv}$ is PV power obtained from MPPT algorithm, V_{gm} is the magnitude of the grid voltage, and $I_{\rm loss}$ is the loss component obtained. The loss component can be regulated by the proposed outer loop controller, which helps to regulate the dc-link voltage and minimize the effect of double-frequency ripple in the generated reference grid current. Furthermore, the generated maximum reference grid current is fed to a robust Lyapunov-based inner loop current controller to achieve fast dynamic response and stability under disturbance with zero steady-state error. However, to achieve high-quality grid current, the resonance damping is essentially for an LCL filter-based system. Therefore, a capacitor voltage loop is accumulated in the proposed control approach, which improves the power quality and assures the global stability of the system.

A. Proposed DC-Link Voltage Control

In the GCPV system, the current is controlled as an inner loop with a higher bandwidth relative to the outer voltage loop. Thus, the dc-link can be modeled as a state variable, considering that it is a single integral plant, which generates the input variable to the current controller. Furthermore, considering u as input and y as an output of dc-link controller, the plant can be represented as

$$\dot{y}(t) = d_i + u \tag{7}$$

where d_i is an input disturbance of the system [28]. In terms of error, the desired output for dc-link controller can be written as

$$\dot{x}_4 = -d_i - u. \tag{8}$$

In the closed-loop system, with the presence of the disturbance d_i, for the absolute tracking of the reference, the control logic must satisfy that $x_4(t) \to 0$ when $t \to \infty$ in a closed-looped system. Thus, a standard PI controller can be usually employed as

$$u_c(t) = k_p x_4 + k_i \int x_4 dt \tag{9}$$

where proportional and integral gains are represented by k_p and k_i, respectively. Using the standard control design methods such as Bode diagram and pole placement with optimization, the voltage control loop can be tuned [17]. However, due to 90° phase lag of the integrator, it persists the saturation issues, thus affecting the stability of the system. Therefore, the integral gain should be reduced to zero during system transients to obviate overshoot, saturation, and instability.

An NPI-based dc-link voltage control is proposed to accomplish a fast dynamic response. It converges the tracking error x_4 between dc-link voltage, $v_{\rm dc}$, and reference dc-link, $v_{\rm dcref}$, obtained from the MPPT algorithm to zero with lesser overshoot. In the proposed dc-link controller, a nonlinear gain function, fal(x_4), is introduced, which, by using a nonlinear mechanism, allows larger gains with smaller errors and smaller gains with larger errors. This leads to a reduction in steady-state error, high disturbance rejection capability, and robustness of the controller

$$fal(x_4) = \begin{cases} |x_4|^m \text{sgn}(x_4), & |x_4| > \delta_p \\ x_4/\delta_p^{(1-m)}, & |x_4| \le \delta_p \end{cases}, \quad \delta_p > 0 \tag{10}$$

where m is the gain of a nonlinear function fal(x_4), sgn(x_4) is a signum function, and δ_p can be selected to limit the gain of the function fal(x_4). The linear operation of the function fal(x_4) can be accrued with $m = 1$. However, to converge the dc-link error and x_4 to zero in finite duration, the value of m must be less than 1. Therefore, in order to mitigate the bounded disturbance encountered by the nonlinear function fal(x_4), the selection m should be restricted to a narrowed bounded range, i.e., when $0 < m < 1$. Furthermore, it is also possible to achieve zero steady-state error with the function fal(x_4) without using the integral control, i.e., when $m \to 0$. Therefore, to achieve faster convergence, fal(x_4) should operate as a nonlinear gain function by properly selecting gain m (i.e., $0 < m < 1$).

In the presence of external disturbances, by eliminating the phase delay due to integral control, the function fal(x_4) can accomplish an enhanced stability margin and reduce the steady-state error to zero. However, It reduces the controller's sensitivity to noise [28]. Hence, an integral controller is introduced to further lower the gain, during a steady state when the error is small. This can be acquired by a function gal(x_4) defined in the following equation:

$$\text{gal}(x_4) = \begin{cases} 0, & |x_4| > \delta_i \\ x_4, & |x_4| \le \delta_i \end{cases}, \quad \delta_i > 0. \tag{11}$$

By considering the operation of functions in (10) and (11), the modified NPI controller can be deduced as

$$u(t) = \left(G_{k_p} + \int G_{k_i} dt \right) x_4 \tag{12}$$

where $G_{k_p} = k_{p\max}\text{fal}(x_4)$ and $G_{k_i} = k_{i\max}\text{gal}(x_4)$. Furthermore, $k_{p\max}$ and $k_{i\max}$ represent proportional and integral gains, respectively, at their maximum values. The inclusion of nonlinear functions, fal(x_4) and gal(x_4), modifies the standard PI controller gains to G_{k_p} and G_{k_i} [29]. During dynamic response for larger tracking errors, the proposed NPI controller $u(t)$ can attain higher bandwidth. Hence, increase the open-loop gain of

the outer-loop voltage controller for dc-link. This accelerates the dynamic response by limiting the open-loop gain and improves the filtering capacity of double-frequency ripple. However, the output of the NPI controller contains an amount of double-frequency ripple, which can increase the harmonic content in the reference grid current due to x_4. Therefore, an MAF filter is implied [30] to attenuate the low-frequency component in the reference current, as shown in Fig. 2, which can be expressed as

$$u_{\mathrm{MAF}} = \left(\frac{1 - e^{-T_s s}}{T_s s}\right) \tag{13}$$

where T_s is the sampling time, which is considered 25 μs. The MAF can filter the frequency harmonic component without influencing the dc component. Therefore, the total loss component across the dc bus can be described as

$$I_{\mathrm{loss}} = \left(G_{k_p} + \int G_{k_i} dt\right)\left(\frac{1 - e^{-T_s s}}{T_s s}\right) x_4. \tag{14}$$

Thus, dc-link error, x_4, can be modified by the outer loop controller gain given as

$$x_4 = G_k I_{\mathrm{loss}} \tag{15}$$

where G_k is the gain of the outer loop voltage controller, which can help to regulate the dc-link voltage with the nonlinear gain corresponding to the dc-link error signal.

B. Lyapunov Function-Based Current Control

The Lyapunov function-based inner loop current control can achieve global stability around its equilibrium point. The single-stage GCPV system reaches the equilibrium point when the state variables $x_1 = x_2 = x_3 = x_4 = 0$ [31]. Thus, the energy dissipation across the state variables converges to zero.

In a PV-based VSI system with an LCL filter, global stability can be obtained considering the energy stored in the capacitors and inductors, which can be deduced utilizing the Lyapunov stability theorem. The Lyapunov function can be expressed as

$$V(x) = \frac{1}{2}L_i x_1^2 + \frac{1}{2}L_g x_2^2 + \frac{1}{2}C x_3^2 + \frac{1}{2}C_{\mathrm{dc}} x_4^2. \tag{16}$$

As (16) is a positive definite scalar function, according to the Lyapunov direct method, the GCPV system is considered to achieve global stability when the derivative of (16) is a negative definite

$$\dot{V}(x) = x_1 L_i \dot{x}_1 + x_2 L_g \dot{x}_2 + x_3 C \dot{x}_3 + x_4 C_{\mathrm{dc}} \dot{x}_4. \tag{17}$$

Substituting (4) into (17) gives

$$\begin{aligned}\dot{V}(x) = {} & x_1(\Delta s_u v_{\mathrm{dc}} - v_c - r_i i_i) + x_2(v_c - r_g i_g - v_g) \\ & + x_3(i_i - i_g) + x_4(i_{\mathrm{pv}} - \Delta s_u i_i).\end{aligned} \tag{18}$$

Applying the defined state variable from (3), we can get

$$\dot{V}(x) = \Delta s_u\left(v_{\mathrm{dcref}} x_1 - i_{\mathrm{iref}} x_4\right) - x_1^2 r_1 - x_2^2 r_2. \tag{19}$$

When the estimated system parameters match the actual values, $\dot{V}(x)$ is always negatively rendered that the perturbed control input can be selected as

$$\Delta s_u = -\alpha_i\left(v_{\mathrm{dcref}} x_1 - i_{\mathrm{iref}} x_4\right) \tag{20}$$

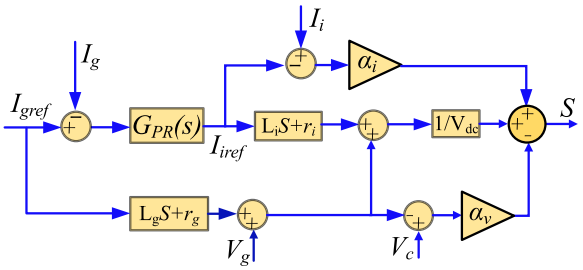

Fig. 4. Lyapunov-based inner loop control structure.

where α_i is a positive scalar gain, i.e., $\alpha_i > 0$ such that Δs_u becomes a negative coefficient. However, under parametric uncertainties, the selected value of α_i should be large enough to dominate (19) to $\dot{V}(x)$ become negative definite. Thus, by considering (20), the switching function s_u can be obtained as

$$s_u = S_u + \alpha_i\left(i_{\mathrm{iref}} x_4 - v_{\mathrm{dcref}} x_1\right) \tag{21}$$

where

$$S_u = \frac{1}{V_{\mathrm{dcref}}}\left(L_i \frac{di_{\mathrm{iref}}}{dt} + r_i i_{\mathrm{iref}} + v_{\mathrm{cref}}\right). \tag{22}$$

In a closed-loop single-phase GCPV system, (22) can assure global stability. However, to mitigate the steady-state error in the grid current due to parametric perturbations and minimize the effect of a differentiator, a PR controller $G_{\mathrm{PR}}(s)$ can be implied [31]

$$G_{\mathrm{PR}}(s) = K_p + \frac{2K_r \omega_c s}{s^2 + 2\omega_c s + \omega^2} \tag{23}$$

where ω and ω_c are the natural frequency and cutoff frequency, respectively. The PR controller reduces the steady-state error to zero and generates the reference inverter current, as shown in Fig. 4

$$I_{\mathrm{iref}} = \frac{K_p s^2 + 2\omega_c(K_p + K_r)s + K_p \omega^2}{s^2 + 2\omega_c s + \omega^2} x_2. \tag{24}$$

Although (21) with PR controller can achieve global stability, it is incorrigible to dampen out the effect of the resonance due to only inverter-side current compensation. Therefore, for achieving the damping in the grid current, (20) can be modified by including the capacitor voltage error (x_3)

$$\Delta s = -\alpha_i(v_{\mathrm{dcref}} x_1 - i_{\mathrm{iref}} x_4) - \alpha_v x_3 \tag{25}$$

where α_v is a capacitor voltage feedback gain. The effect of the double-frequency ripple, present in the dc-link error, x_4, can be minimized by an NPI with MAF control, which modifies the grid current reference in (25) to obtain (26). Thus, the final switching function can be obtained as (26), and the control logic is shown in Fig. 4

$$s_u = S_u - \alpha_i(v_{\mathrm{dcref}} x_1 - i_{\mathrm{iref}} x_4) - \alpha_v x_3. \tag{26}$$

C. Design Guideline

The proposed nonlinear controller is composed of standard PI parameters $k_{p\max}$ and $k_{i\max}$ and nonlinear functions $\mathrm{fal}(x_4)$ and $\mathrm{gal}(x_4)$, which include the selection of m, δ_p, and δ_i.

The design approach required tuning the gain of the standard PI controller for desired dc-link voltage dynamics, which can be considered as the maximum the tuned gains $k_{p\max}$ and $k_{i\max}$. Furthermore, the design approach is done by theoretically analyzing the parameter selection depending upon the behavior of the nonlinear functions on different values within a limited range [18], [28].

The gain factor m can be selected such that $0 < m < 1$ yields a high gain when the dc-link error is small and a low gain for the higher value of error. It ameliorates the dynamic performance and tends to achieve zero steady-state error in dc-link. The selection of δ_p for the function $\text{fal}(x_4)$ can preclude the chattering phenomenon by limiting the gain to $k_{p\max}/\delta_p^{(m-1)}$ [32]. However, to incorporate an integral control during steady state (i.e., during small error), a function $\text{gal}(x_4)$ is applied by adjusting the value of δ_i (selected as $\delta_i < \delta_p/10$), which further restrains the gain of the NPI controller. The optimum adjustment of the gain related to $\text{fal}(x_4)$ and $\text{gal}(x_4)$ can ameliorate the transient performance and disturbance rejection ability. The selection of $k_{p\max} = 55$ and $k_{i\max} = 0.001$ is similar to the conventional PI control discussed in [17], considering the gain of the nonlinear function $m = 1$. Furthermore, to improve the performance of the dc-link voltage control, the parameters of the NPI controller are selected as $m = 0.325$, $\delta_p = 0.214$, and $\delta_i = 0.01$.

The outer loop dc-link controller has a similar tuning method to standard PI control dc-link voltage with improved dynamic performance and high disturbance rejection. Therefore, the proposed controller can directly replace the standard PI controller after selecting the bounded limit for m (i.e., $0 < m < 1$).

The inner loop current controller design guideline depends upon the selection of α_i and α_v gains, as described in [31]. The proper selection of the gains corresponds to a fast dynamic response and lesser harmonics response in the grid current. Thus, the optimum value of α_i can achieve low current harmonics and provide global stability to the GCPV system. However, proper selection of α_v can achieve resonance damping in the grid current. Therefore, by the analysis of the root locus of the dominant closed-loop poles, the optimum values of α_i and α_v are selected as -0.0023 and 0.287, respectively.

The design of the dc-link voltage controller also depends on the proper selection of dc-link capacitor C_{dc} [17], [23], which regulates the dc ripple around a reference value. The dc-link capacitors can be chosen as

$$C_{\text{dc}} \geq \frac{P_g}{2\omega_g V_{\text{dc}} \delta v_{\text{dc}}} \tag{27}$$

where ω_g is the grid angular frequency, δv_{dc} is the dc-link ripple, and P_g is the power injected into the grid. The capacity of the dc-link capacitor, C_{dc}, helps to reduce ripple voltage and vice versa. When C_{dc} is large, however, the size, weight, and cost of the converter increase.

D. Stability Analysis

The stability of the proposed controller (26) can be defined by the stability of the Lyapunov-based inner loop control and the NPI-based outer loop control, operating as a cascaded control structure. The stability of the outer loop control $u(t)$ can be defined by the stability of the proportional control $G_{k_p} = k_{p\max}\text{fal}(x_4)$, which contains a nonlinear function $\text{fal}(x_4)$, as described in (10). In the NPI controller plant (8), the disturbance w can be ignored for the sake of simplicity of the stability analysis. Then, the final effective nonlinear feedback control, without limiting the gain of the controller, can be written as

$$u(t) = -k_{p\max}|x_4|^m \text{sgn}(x_4). \tag{28}$$

The proposed control law in (28) can guarantee the asymptotic stability of the closed-loop system when $k_{p\max}$ is selected such that [28]

$$k_{p\max} > \sup_{x_4}\left(\frac{|f(x_4)|}{|x_4|^m}\right) \tag{29}$$

considering the plant of the system unknown and $f(x_4)$ as the accounts for the nonlinear dynamics of x_4 in the system. To validate the above, a Lyapunov function $V(x_4) = x_4^2/2$ is selected. Then, the derivative of $V(x_4)$ can be

$$\begin{aligned}\dot{V}(x_4) &= x_4\dot{x}_4 = -x_4 f(x_4) - k_{p\max}x_4|x_4|^m \text{sgn}(x_4)\\ &= -x_4 f(x_4) - k_{p\max}|x_4|^{m+1}.\end{aligned} \tag{30}$$

As per Lyapunov stability theorem, the stability of the system can be achieved when (30) satisfies the following conditions.

1) If $x_4 f(x_4) \geq 0$, and $k_{p\max} > 0$, then $s\dot{V}(x_4) < 0$ for $x_4 \neq 0$.
2) If $x_4 f(x_4) < 0$, and $k_{p\max} > 0$ then for $\dot{V}(x_4) < 0$ $k_{p\max}|x_4|^{m+1} > |x_4 f(x_4)|$, or equivalent to (29).

Therefore, the asymptotic stability of the closed-loop control law (28) can be defined by the proper selection of the controller gains $k_{p\max}$ and m.

The stability of the inner loop Lyapunov-based controller can be determined by the closed-loop transfer function of the reference grid current to the actual grid current [31]. Linearizing (1), (3), and (26) around the equilibrium point can give the characteristic in the following equation:

$$A_5 s^5 + A_4 s^4 + A_3 s^3 + A_2 s^2 + A_1 s^1 + A_0 = 0 \tag{31}$$

where

$$\begin{aligned}A_5 &= C_{\text{dc}} L_i L_g C\\ A_4 &= 2\omega_c L_i L_g C - L_g C C_{\text{dc}}\alpha_i V_{\text{dcref}}^2\\ A_3 &= L_i + L_g + \omega L_i L_g C - 2\omega_c L_g C C_{\text{dc}}\alpha_i V_{\text{dcref}}^2\\ &\quad \times L_i K_p + L_g \alpha_v C_{\text{dc}} V_{\text{dcref}}\\ A_2 &= 2\omega_c(L_i K_p + L_i K_r + L_i + L_g + L_g\alpha_v V_{\text{dcref}})\\ &\quad - \alpha_i C_{\text{dc}} V_{\text{dcref}}^2(1 + K_p + \omega^2 L_g C)\\ A_1 &= \omega^2(L_i + L_g + L_i K_p + L_g\alpha_v V_{\text{dcref}})\\ &\quad - 2\omega_c\alpha_i C_{\text{dc}} V_{\text{dcref}}^2(K_p + K_r + 1)\end{aligned}$$

and $A_0 = -\omega\alpha_i C_{\text{dc}} V_{\text{dcref}}^2(1 + K_p)$. It is clear that all coefficients of the characteristic equation are positive constants, considering that $\alpha_i < 0$, $\alpha_v > 0$, $K_p > 0$,

TABLE I
PARAMETERS FOR SIMULATION AND EXPERIMENT

PV system parameters	
Series (N_{se}) and parallel panels (N_p)	14 and 1
Open circuit voltage (v_{oc})	37.1 V
Maximum voltage (v_{pv})	29.6 V
Short circuit current (i_{sc})	8.26 A
Maximum current (i_{pv})	7.6 A
Peak power (p_{pv})	224.96 W
Output power at MPP (P_{pv})	3.1 kW
GCI system parameters	
Sampling and Switching frequency (T_s, f_s)	40 kHz, 10 kHz
Grid Voltage and frequency (V_g, f_g)	230 V, 50 Hz
DC-link Capacitor (C_{dc})	1100 μF
Filter Capacitor (C)	50 μF
Filter inductors (L_g, L_i)	0.33 mH, 3.3 mH
Internal resistance (r_i, r_g)	0.7 Ω, 0.3 Ω
Grid impedance (Z_g)	0.1 Ω, 0.25 mH

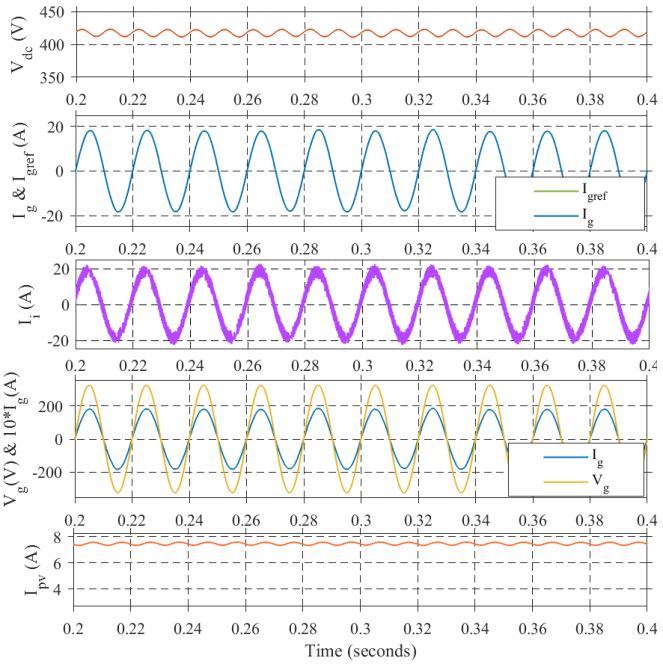

Fig. 5. Simulation results showing performance of the proposed controller in steady state while transferring rated power into the grid at upf.

and $K_r > 0$. Therefore, all poles are positioned in the left half of the s-plane if $A_1A_4 - A_0A_5 > 0$, $A_3A_4 - A_2A_5$ and $(A_3A_4 - A_2A_5)[A_1A_2A_4 - A_0A_5(A_2 + A_4)] + (A_1A_4 - A_0A_5)(A_0A_4A_5 - A_1A_4^2) > 0$ are satisfied. Hence, by selecting the proper gains of the controller, stability can be ensured to satisfy the above conditions.

IV. RESULTS AND DISCUSSION

Tests of the proposed controller are conducted in MATLAB and experimentally verified with the dSPACE MicroLabBox-based platform against the PV array, grid, and load disturbances. The detailed parameters related to the PV array and single-stage single-phase GCPV system with an LCL filter are presented in Table I.

A. Simulation Results

1) Performance Under Steady State and Perturbation of Solar Irradiance: Fig. 5 shows the performance of

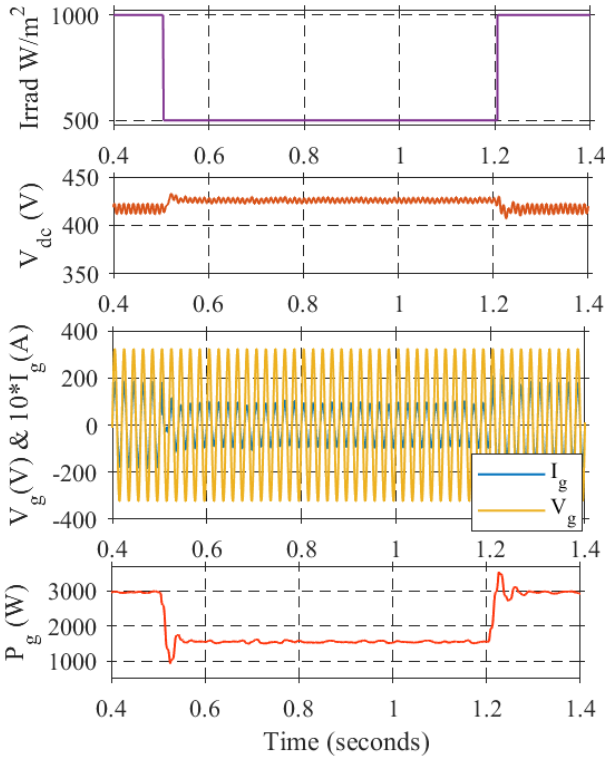

Fig. 6. Simulation results showing dynamic performance of GCPV system with PV-side disturbances.

single-stage GCPV in a steady state at PV irradiance of 1000 W/m^2 at 25°. At the point of common coupling (PCC), the grid current i_g remains in phase with grid voltage v_g under the upf operation. It can be observed that the inverter current, i_i, has high harmonics, which is further minimized in generated grid current i_{gref}. The proposed Lyapunov-based inner loop controller shows that the grid current i_g tracks the reference grid current i_{gref} and diminishes the steady-state error to zero. With an active power of 3 kW, a peak grid current of 18.23 A (13 A rms) is fed into the grid at a THD of 1.34%. The active damping employed can eliminate the effect of resonance. However, the effect of double line frequency on grid current, i_g, can be mitigated by the proposed NPI with an MAF and proceeds with a stable dc-link voltage.

Fig. 6 shows the performance of the proposed controller under perturbation of the solar irradiance, considering a step change from 1000 to 500 W/m^2 and 500 to 1000 W/m^2 at 25°. The proposed NPI controller shows faster dynamics with change in irradiance, which keeps the dc-link stable. The dc-link voltage shows the fast convergence on a timescale of 60 ms for both step-up and step-down changes in irradiance. The proposed dc-link controller can conveniently suppress the disturbances due to the power change on the PV side. As shown in the zoomed-in view in Fig. 7, with the fast convergence of the dc-link, the grid current i_g becomes stable within one cycle to ensure the stability of the GCPV system. The sudden change in irradiance at 0.505 s reduces the grid current to 9.5 A (peak value), as shown in Fig. 7, which increases the THD to 2.43%. However, it is under

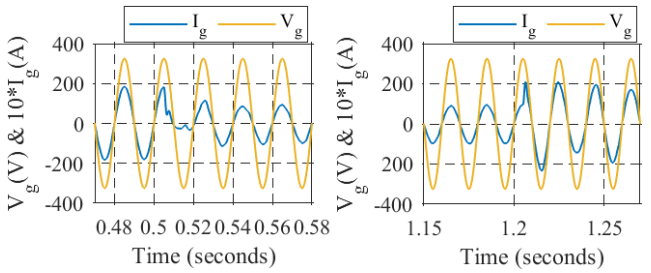

Fig. 7. Zoomed-in view showing the grid current and grid voltage under step change in irradiance.

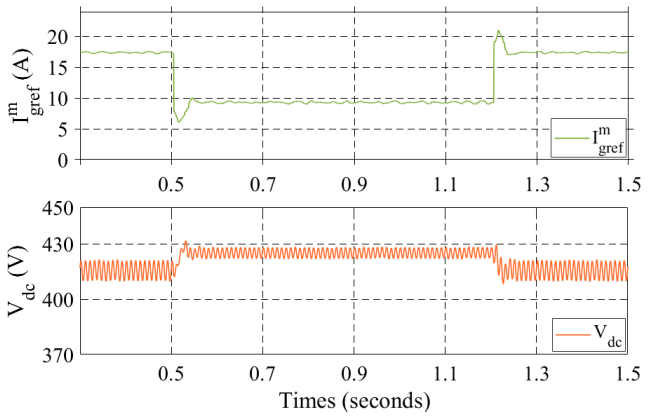

Fig. 8. Zoomed-in view of proposed NPI controller performance, showing reference grid current and dc-link voltage.

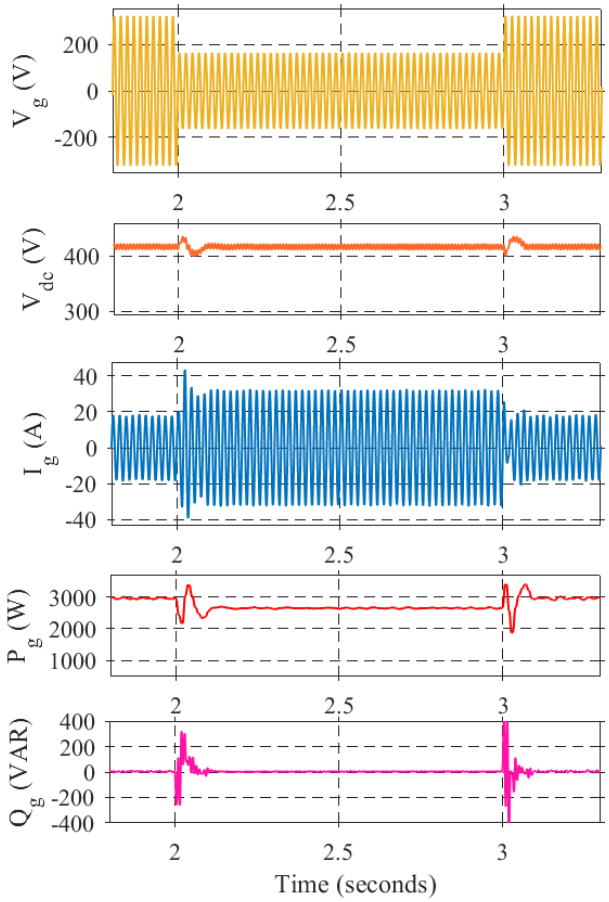

Fig. 9. Simulation results showing the performance of the controller under grid-side disturbances, considering 50% voltage sag in the grid voltage.

the acceptable range of IEEE standard 1547–2003. Moreover, as shown in Fig. 8, the magnitude of the reference grid current I^m_{gref} generated does not contain any second harmonic oscillation due to the presence of double-frequency ripple in the dc-link.

2) Performance Under Grid-Side Disturbances: The robustness of the proposed controller to the grid disturbances is observed, as shown in Fig. 9. A voltage sag of 50% is considered for a duration of 1 s in the grid voltage at PCC. Under severe grid disturbance, the dc-link voltage V_{dc} is stable, and the grid current I_g has a low ripple with the upf operation. An increase in the grid current is due to the decrease in voltage at PCC, which keeps the input PV voltage and output active power feeding into the grid balanced. The dc-link voltage across the inverter is stable at the maximum power generated from the PV system. However, the current across the inverter increases to achieve maximum power transfer with no reactive power, Q_g compensation into the grid. Furthermore, a reduction in load current can be assumed to compensate for the power.

Moreover, with the increase in the grid current, the active power P_g decreases due to higher losses across the inverter and filter resistance. It can be observed that the grid current can be increased between 2 and 3 s and has a %THD of 0.52%. The dc-link fluctuation settled within 80 ms with an overshoot of 10 V. The grid current is stable during the disturbance and restored to normal under three cycles during grid voltage fluctuation.

3) Performance Under Sudden Connection and Disconnection of Local Load: The dynamic response under sudden load connection and disconnection of 2.1-kW local load at PCC is tested. The proposed controller keeps the dc-link stable and the PV integrated system synchronized with the grid, as shown in Fig. 10. However, a step change in load causes a steep change in grid current, with an increase in the grid current THD to 3.12% from 1.34% during steady state, which is under IEEE standard 1547. The load transient gets settled instantly, and the power transfers from solar PV to the local load at PCC. Therefore, the active transfer to the grid is reduced to 900 W. Moreover, the grid current is still tracking the reference at upf without having a stability problem. It is observed that when the generated capacity is higher than the household consumption or local load, the generated excess power is considered to be exported into the grid.

4) Performance With Variation in Filter Parameters and Grid Impedance: Fig. 11(a) exhibits the steady-state performance of the grid current and voltage with +20% variation in LCL-filter parameters. The grid current is still in phase with the grid voltage, while the rated power is transferred into the grid. The proposed NPI with the Lyapunov controller shows robustness to parameter uncertainties. Moreover, in Fig. 11(b), the performance of the system with grid impedance variation at PCC is tested. The grid voltage and current are in phase with each other when the grid inductance, Z_g, changes from 0.25 to 2.25 mH.

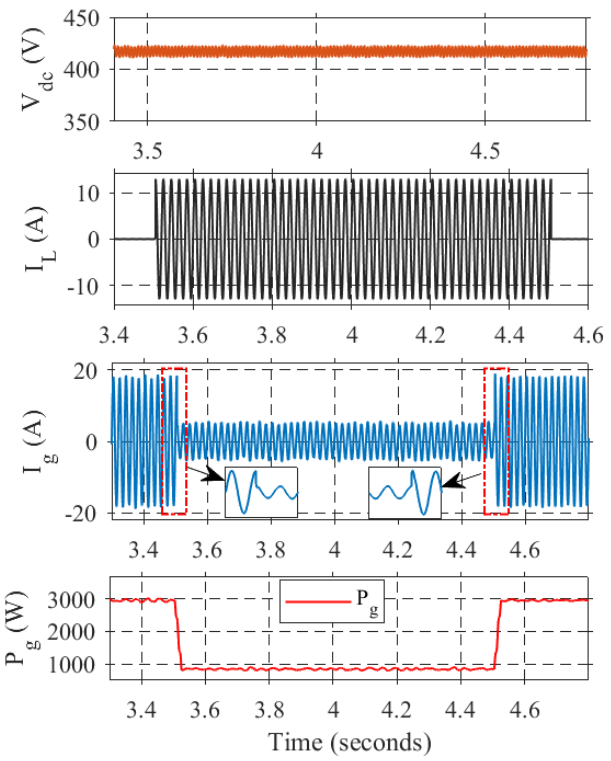

Fig. 10. Performance of the controller under sudden connection and disconnection of the local load at PCC.

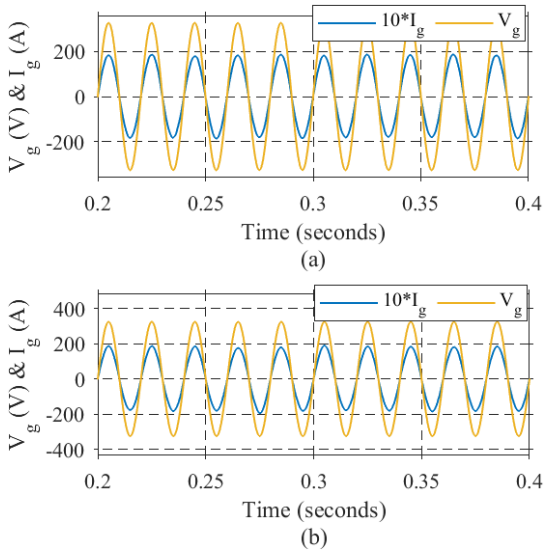

Fig. 11. Simulation results showing the robustness of the controller under parametric uncertainties. (a) Considering 20% change in filter parameter and (b) with high grid impedance ($Z_g = 0.1\ \Omega$, 4.25 mH).

B. Experimental Results

Experimental analysis on a hardware testbed consists of Semikron inverter switches SKM100GB063D with LV25 voltage and HX 25-P current sensors. The complete setup and block representation of the connection for experimental platform is shown in Fig. 12. The controller was compiled into a dSPACE MicroLabBox for generating the switching pulses at a sampling period of 25 μs.

1) Performance Under PV-Side Disturbances: The performance of the proposed controller is validated under PV-side

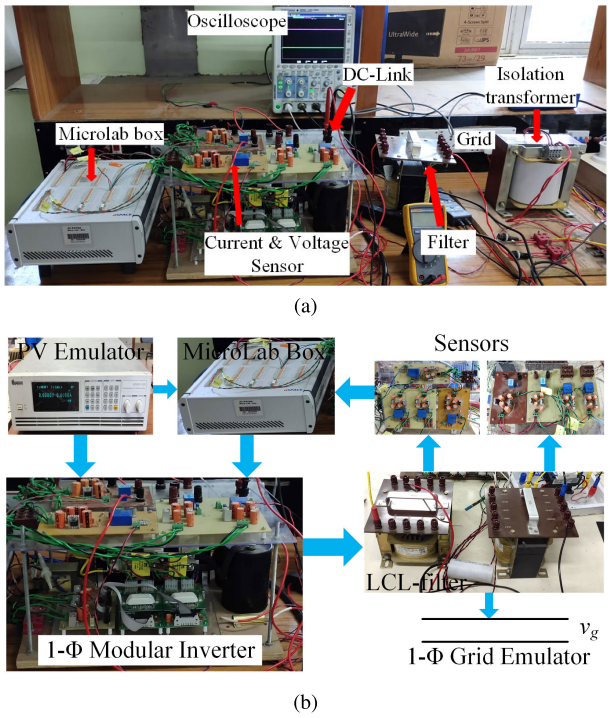

Fig. 12. Experimental platform for single-stage system. (a) Complete setup. (b) Block representation of the connection.

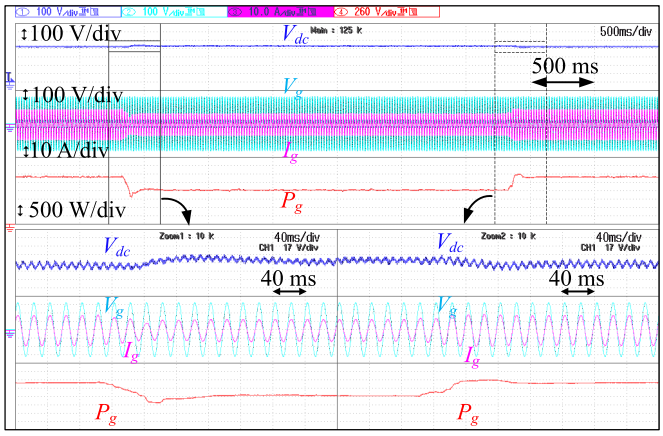

Fig. 13. Experimental result showing the robustness of the controller under PV intermittency of 1000–700 W/m^2.

disturbance, considering a sudden change in irradiance, as shown in Fig. 13. The proposed controller sustains the stability of the dc-link for a ramp change in irradiance from 1000 to 700 W/m^2 and then to 1000 W/m^2. The proposed NPI controller with MAF shows a fast transient period of 80 ms with a lesser overshoot of 4.7%. Despite input PV power fluctuations, the fast convergence of the proposed dc-link controller ensures the stability and robustness of the system. Moreover, it mitigates the double-frequency ripple. Hence, transfer high-quality power with current THD of 1.4% and 2.03% in 1000 and 700 W/m^2, respectively. Furthermore, it prevents phase deviation and reduces the third harmonic injection.

2) Performance Under Grid-Side Disturbances: The disturbance rejection capability of the proposed controller is tested

TABLE II
COMPARATIVE ANALYSIS

Aggregation	Proposed Controller	[33]	[21]	[25]	[20]	[14]	[23]	[27]
Computational burden	medium	medium	medium	high	medium	high	high	medium
% THD of i_g	1.34%	2.49%	NR	3.92%	4.5%	2.54%	2.06%	1.93%
% voltage ripple at DC-bus	2.6%	5.3%	4.2%	3%	5.5%	12%	1.2%	4%
% Overshoot in DC-bus	3%	7.5%	2%	5%	5.5%	15%	3%	3.5%
Controller	NPI + Lyapunov	pq+HCC	feedback linearization	ST-SM + AQ-PR	Adaptive PI	H_∞ + μ-synthesis	PR+SMC	PI+HCC
Switching frequency f_{sw}	10 kHz	10 kHz	10 kHz	5 kHz	20 kHz	40 kHz	20 kHz	8.5 kHz
i_g response (t_s in cycles)	1.5	5	3.5	3.5	3	2	2	1.5
Filter utilized	LCL	LC	LCL	L	L	LCL	L	LCL

*NR = Not Reported

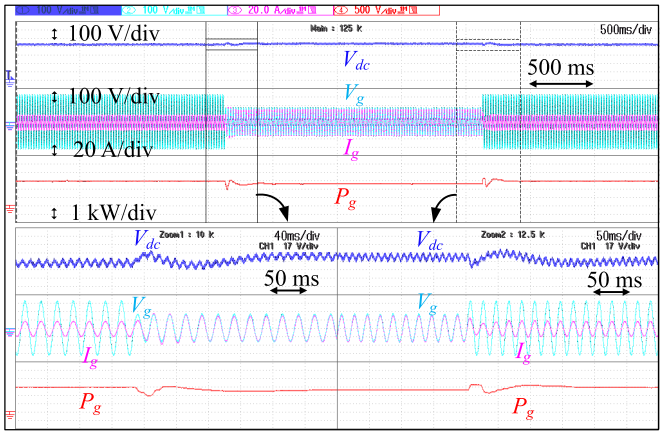

Fig. 14. Experimental result showing the robustness of the controller under 50% voltage sag.

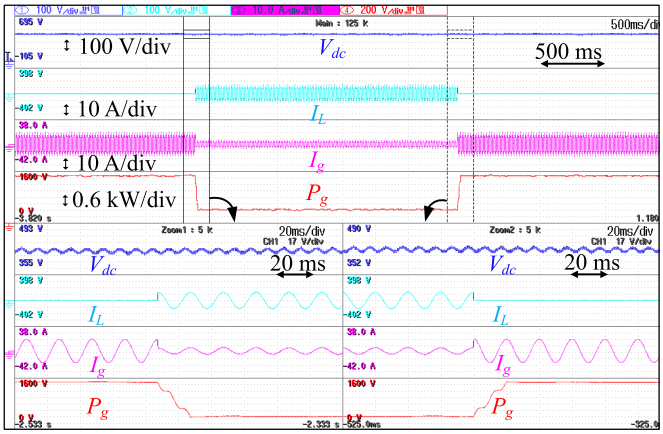

Fig. 15. Experimental result exhibits the robustness of the proposed controller under sudden connection and disconnection of 2.1-kW load.

under grid disturbance, considering a 50% voltage sag in the grid voltage at PCC. In Fig. 14, it can be seen that with the sudden voltage sag, the dc-link is kept stable at MPP by the proposed controller with a maximum overshoot of 3.5% and a transient period of 110 ms. Moreover, by eliminating the effect of phase shift due to dc-link ripple in single-stage single-phase GCPV systems, the grid current and voltage are in phase, which gives the upf operation. Moreover, to maintain grid-to-PV power balance during voltage sag periods, the grid current increases.

3) Performance With the Sudden Change in the Local Load: The dynamics of the proposed controller are tested with sudden connection and disconnection of 2.1-kW local load, as shown in Fig. 15. The load current I_L, grid current I_g, power feeding into the grid P_g, and the dc-link voltage $V_{\rm dc}$ are exhibited to present the dynamic performance. When a load transient of 2.1 kW is employed, it introduces a steep change in the grid current. However, the proposed controller maintains the stability of the system under load disturbances. During a load change of 2.1 kW, a change from 3 kW to 900 W can be detected in power feeding into the grid, which increases the grid current THD to 3.34%. However, with the proposed controller, it is under IEEE standard 1547. Moreover, due to the proposed controller, conserving the stability of the system at MPP during load disturbance, the dc-link voltage does not show any change.

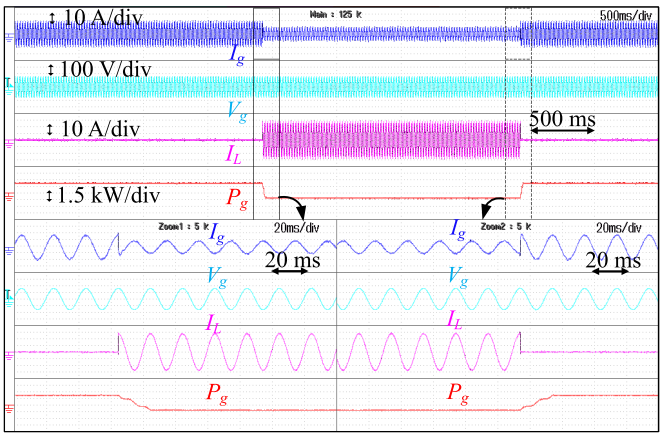

Fig. 16. Experimental result exhibits the robustness of the proposed controller under sudden connection and disconnection of 4.5-kW load.

Fig. 16 shows the effect of the sudden connection of a 4.5-kW load, which is higher than the maximum available PV power of 3 kW. The controller, ensuring the stability of the GCPV system, allows a negative power of 1.5 kW

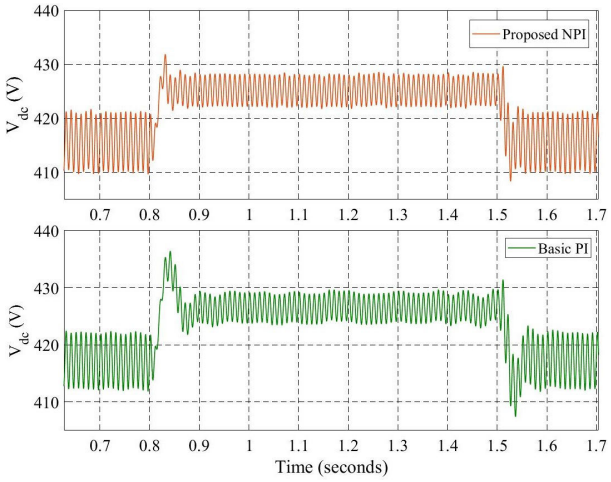

Fig. 17. Performance of dc-link controller under a change in irradiance with NPI and basic PI controller.

to the local load. The sudden higher loading forces the grid current I_g and 180° phase difference with the grid voltage V_g.

C. Comparative Performance Evaluation

A comparative performance evaluation is studied in Table II with existing state-of-the-art literature [14], [20], [21], [23], [25], [27], [33]. The proposed controller for the single-phase single-stage GCPV system has a minimum current THD of 1.34%. Moreover, the grid current settled in 1.5 cycles with a lesser overshoot of 3%, which is faster than its counterpart due to the NPI-based controller in conjunction with the Lyapunov controller. It has comparably equal performance to the [23]; however, [23] utilizes a passive LC resonant circuit across dc-link as an external hardware to eliminate the double-frequency ripple. Moreover, it has two extra switches than the conventional single-phase system and has a higher switching frequency, which can increase the overall power loss across the converter. Fig. 17 shows a comparative performance of the dc-link controller under a change in irradiance from 1000 to 500 W/m^2 at 0.805 s and 500–1000 W/m^2 at 1.505 s. Both NPI and basic PI controllers maintain the dc-link voltage stability with sudden changes. However, the proposed NPI has a settling time of 60 ms, which is faster than the standard PI controller of 100 ms. Moreover, with the introduction of MAF, the dc-link ripple is 10 V, which is under the maximum limit of 10% of the rated voltage across the capacitor. It is well observed that the proposed controller can effectively address the major issues of the single-phase single-stage GCPV system.

V. Conclusion

A robust cascaded nonlinear controller is proposed to improve the performance of the grid current for a single-phase single-stage GCPV system with an LCL filter. In the case of both internal and external disturbances, the inner loop Lyapunov current controller can ensure global stability and robustness. Moreover, an active damping and zero steady-state error can also be accomplished. Furthermore, the proposed nonlinear controller for outer loop control has fast dynamic performance against external disturbances. The inclusion of an MAF filter eliminates the effect of double-frequency ripple and reduces the harmonics in grid current. Therefore, the combination of the proposed outer loop controller with filter and feedforward term improves the dc-link voltage regulation and compensates for the phase delay. With a high gain for lower error values and a low gain for high error values, it can ensure robustness and stability against PV-side disturbances. Furthermore, a robust inner loop controller with cohesion of the proposed outer loop eliminates the effect of phase shift in the grid current and improves the power quality. A hardware testbed with the proposed controller tested the effectiveness under various PV- and grid-side disturbances. Hence, the proposed controller can be recommended for single-phase rooftop PV to the grid-integrated system.

References

[1] J. M. Carrasco et al., "Power-electronic systems for the grid integration of renewable energy sources: A survey," *IEEE Trans. Ind. Electron.*, vol. 53, no. 4, pp. 1002–1016, Jun. 2006.

[2] G. Petrone, G. Spagnuolo, R. Teodorescu, M. Veerachary, and M. Vitelli, "Reliability issues in photovoltaic power processing systems," *IEEE Trans. Ind. Electron.*, vol. 55, no. 7, pp. 2569–2580, Jul. 2008.

[3] R. Panigrahi, S. K. Mishra, S. C. Srivastava, A. K. Srivastava, and N. N. Schulz, "Grid integration of small-scale photovoltaic systems in secondary distribution network—A review," *IEEE Trans. Ind. Appl.*, vol. 56, no. 3, pp. 3178–3195, May 2020.

[4] M. Zhao, X. Yuan, J. Hu, and Y. Yan, "Voltage dynamics of current control time-scale in a VSC-connected weak grid," *IEEE Trans. Power Syst.*, vol. 31, no. 4, pp. 2925–2937, Jul. 2016.

[5] H. Yuan, X. Yuan, and J. Hu, "Modeling of grid-connected VSCs for power system small-signal stability analysis in DC-link voltage control timescale," *IEEE Trans. Power Syst.*, vol. 32, no. 5, pp. 3981–3991, Sep. 2017.

[6] Z. Yang, R. Ma, S. Cheng, and M. Zhan, "Nonlinear modeling and analysis of grid-connected voltage-source converters under voltage dips," *IEEE J. Emerg. Sel. Topics Power Electron.*, vol. 8, no. 4, pp. 3281–3292, Dec. 2020.

[7] J. Roldán-Pérez, E. J. Bueno, R. Pe na-Alzola, and A. Rodríguez-Cabero, "All-pass-filter-based active damping for VSCs with LCL filters connected to weak grids," *IEEE Trans. Power Electron.*, vol. 33, no. 11, pp. 9890–9901, Nov. 2018.

[8] M.-S. Karbasforooshan and M. Monfared, "Adaptive self-tuned current controller design for an LCL-filtered LC-tuned single-phase shunt hybrid active power filter," *IEEE Trans. Power Del.*, vol. 37, no. 4, pp. 2747–2756, Aug. 2022.

[9] S. G. Parker, B. P. McGrath, and D. G. Holmes, "Regions of active damping control for LCL filters," *IEEE Trans. Ind. Appl.*, vol. 50, no. 1, pp. 424–432, Jan. 2014.

[10] M. P. Kazmierkowski and L. Malesani, "Current control techniques for three-phase voltage-source PWM converters: A survey," *IEEE Trans. Ind. Electron.*, vol. 45, no. 5, pp. 691–703, 1998.

[11] J. Khazaei, Z. Tu, A. Asrari, and W. Liu, "Nonlinear control design for voltage source converters in weak AC grids," in *Proc. IEEE Texas Power Energy Conf. (TPEC)*, Feb. 2020, pp. 1–6.

[12] M. A. Mahmud, H. R. Pota, and M. J. Hossain, "Nonlinear current control scheme for a single-phase grid-connected photovoltaic system," *IEEE Trans. Sustain. Energy*, vol. 5, no. 1, pp. 218–227, Jan. 2014.

[13] M. A. Mahmud, M. J. Hossain, H. R. Pota, and N. K. Roy, "Robust nonlinear controller design for three-phase grid-connected photovoltaic systems under structured uncertainties," *IEEE Trans. Power Del.*, vol. 29, no. 3, pp. 1221–1230, Jun. 2014.

[14] N. Amouzegar Ashtiani, S. M. Azizi, and S. A. Khajehoddin, "Robust control design for high-power density PV converters in weak grids," *IEEE Trans. Control Syst. Technol.*, vol. 27, no. 6, pp. 2361–2373, Nov. 2019.

[15] X. Shen et al., "Adaptive second-order sliding mode control for grid-connected NPC converters with enhanced disturbance rejection," *IEEE Trans. Power Electron.*, vol. 37, no. 1, pp. 206–220, Jan. 2022.
[16] X. Zhou, Q. Liu, Y. Ma, and B. Xie, "DC-link voltage research of photovoltaic grid-connected inverter using improved active disturbance rejection control," *IEEE Access*, vol. 9, pp. 9884–9894, 2021.
[17] M. Karimi-Ghartemani, S. A. Khajehoddin, P. Jain, and A. Bakhshai, "A systematic approach to DC-bus control design in single-phase grid-connected renewable converters," *IEEE Trans. Power Electron.*, vol. 28, no. 7, pp. 3158–3166, Jul. 2013.
[18] J. Honkanen, J. Hannonen, J. Korhonen, N. Nevaranta, and P. Silventoinen, "Nonlinear PI-control approach for improving the DC-link voltage control performance of a power-factor-corrected system," *IEEE Trans. Ind. Electron.*, vol. 66, no. 7, pp. 5456–5464, Jul. 2019.
[19] R. Errouissi, A. Al-Durra, and S. M. Muyeen, "Design and implementation of a nonlinear PI predictive controller for a grid-tied photovoltaic inverter," *IEEE Trans. Ind. Electron.*, vol. 64, no. 2, pp. 1241–1250, Feb. 2017.
[20] M. Merai, M. W. Naouar, I. Slama-Belkhodja, and E. Monmasson, "An adaptive PI controller design for DC-link voltage control of single-phase grid-connected converters," *IEEE Trans. Ind. Electron.*, vol. 66, no. 8, pp. 6241–6249, Aug. 2019.
[21] L. Callegaro, C. A. Rojas, M. Ciobotaru, and J. E. Fletcher, "A controller improving photovoltaic voltage regulation in the single-stage single-phase inverter," *IEEE Trans. Power Electron.*, vol. 37, no. 1, pp. 354–363, Jan. 2022.
[22] S. Taghizadeh, M. Karimi-Ghartemani, M. J. Hossain, and J. Lu, "A fast and robust DC-bus voltage control method for single-phase voltage-source DC/AC converters," *IEEE Trans. Power Electron.*, vol. 34, no. 9, pp. 9202–9212, Sep. 2019.
[23] B. Guo et al., "Optimization design and control of single-stage single-phase PV inverters for MPPT improvement," *IEEE Trans. Power Electron.*, vol. 35, no. 12, pp. 13000–13016, Dec. 2020.
[24] Y. Shi, B. Liu, and S. Duan, "Modelling, control and performance analysis of a single-stage single-phase inverter with reduced low-frequency input current ripple," *IET Power Electron.*, vol. 11, no. 6, pp. 1074–1082, May 2018. [Online]. Available: https://ietresearch.onlinelibrary.wiley.com/doi/abs/10.1049/iet-pel.2017.0646
[25] J. Xia, Y. Guo, X. Zhang, J. Jatskevich, and N. Amiri, "Robust control strategy design for single-phase grid-connected converters under system perturbations," *IEEE Trans. Ind. Electron.*, vol. 66, no. 11, pp. 8892–8901, Nov. 2019.
[26] D. Pal and B. K. Panigrahi, "A nonlinear adaptive stabilizing control strategy to enhance dynamic stability of weak grid-tied VSC system," *IEEE Trans. Power Del.*, vol. 37, no. 3, pp. 2182–2193, Jun. 2022.
[27] J. K. Singh, K. A. Jaafari, R. K. Behera, K. A. Hosani, and U. R. Muduli, "Faster convergence controller with distorted grid conditions for photovoltaic grid following inverter system," *IEEE Access*, vol. 10, pp. 29834–29845, 2022.
[28] Z. Gao, "From linear to nonlinear control means: A practical progression," *ISA Trans.*, vol. 41, no. 2, pp. 177–189, Apr. 2002.
[29] J. K. Singh, S. Prakash, and R. K. Behera, "A nonlinear loop filter based PLL with harmonic filtering capability for single-phase grid integrated system with improved dynamic performance," *IEEE Trans. Power Del.*, vol. 37, no. 6, pp. 4869–4879, Dec. 2022.
[30] S. Golestan, M. Ramezani, J. M. Guerrero, F. D. Freijedo, and M. Monfared, "Moving average filter based phase-locked loops: Performance analysis and design guidelines," *IEEE Trans. Power Electron.*, vol. 29, no. 6, pp. 2750–2763, Jun. 2014.
[31] H. Komurcugil, N. Altin, S. Ozdemir, and I. Sefa, "Lyapunov-function and proportional-resonant-based control strategy for single-phase grid-connected VSI with LCL filter," *IEEE Trans. Indus. Electron.*, vol. 63, no. 5, pp. 2838–2849, May 2016.
[32] J. Han, "From PID to active disturbance rejection control," *IEEE Trans. Ind. Electron.*, vol. 56, no. 3, pp. 900–906, Mar. 2009.
[33] A. Datta, R. Sarker, and I. Hazarika, "An efficient technique using modified *p-q* theory for controlling power flow in a single-stage single-phase grid-connected PV system," *IEEE Trans. Ind. Informat.*, vol. 15, no. 8, pp. 4635–4645, Aug. 2019.

Jitendra Kumar Singh (Member, IEEE) received the B.E. degree in electrical and electronics engineering from BITS, Bhopal, India, in 2010, the M.E. degree in power electronics engineering from the Birla Institute of Technology (BIT) Mesra, Ranchi, India, in 2016, and the Ph.D. degree in electrical engineering from Indian Institute of Technology Patna (IIT), Patna, India, in 2023.

He was a Visiting Scholar with the Department of Electrical Engineering, Khalifa University, Abu Dhabi, United Arab Emirates, in 2022. He is currently with the Department of Wind and Energy Systems, Technical University of Denmark, Roskilde, Denmark. His research interests include control methods for power electronics converters in distribution systems, renewable energy interconnection, control issues in power systems with inverter-based resources (IBRs), stability issues with IBRs, and HVDC.

Khaled Al Jaafari (Senior Member, IEEE) received the B.Sc. and M.Sc. degrees in electrical engineering (EE) from the Petroleum Institute, Abu Dhabi, United Arab Emirates, in 2006 and 2011, respectively, and the Ph.D. degree from the Department of Electrical and Computer Engineering, Texas A&M University, College Station, TX, USA, in 2016.

He has two years (2006–2008) of experience at ZADCO, Abu Dhabi, as an Electrical Engineer at the upper Zakum Oil field platform, where he was part of the site facility and maintenance engineering team. He is currently an Assistant Professor with the Khalifa University of Science and Technology, Abu Dhabi. His research interests include machine condition monitoring, power system analysis, power system protection, and power quality studies.

Hatem H. Zeineldin (Senior Member, IEEE) received the B.Sc. and M.Sc. degrees in electrical engineering from Cairo University, Giza, Egypt, in 1999 and 2002, respectively, and the Ph.D. degree in electrical and computer engineering from the University of Waterloo, Waterloo, ON, Canada, in 2006.

He was with Smith and Andersen Electrical Engineering, Inc., North York, ON, USA, where he was involved in projects, including distribution system designs, protection, and distributed generation. He was a Visiting Professor with Massachusetts Institute of Technology, Cambridge, MA, USA. He is currently with the Khalifa University of Science and Technology, Abu Dhabi, United Arab Emirates, and on leave from the Faculty of Engineering, Cairo University. His current research interests include distribution system protection, distributed generation, and microgrids.

Dr. Zeineldin is an Editor of IEEE TRANSACTIONS ON ENERGY CONVERSION.

Ranjan Kumar Behera (Senior Member, IEEE) received the B.Eng. degree in electrical engineering from the Regional Engineering College Rourkela, Rourkela, India, in 1998, and the M.Tech. and Ph.D. degrees in electrical engineering from Indian Institute of Technology Kanpur, Kanpur, India, in 2003 and 2009, respectively.

Since 2009, he has been a Faculty Member and is currently an Associate Professor with the Department of Electrical Engineering, Indian Institute of Technology Patna, Patna, India. His research interests include nonlinear control theory application to power electronic converters, pulsewidth modulation techniques, and multiphase electric drive control.

Dr. Behera was a recipient of the 2022 IEEE Outstanding Paper Award for IEEE TRANSACTIONS ON INDUSTRIAL ELECTRONICS.

Ahmed Al-Durra (Senior Member, IEEE) received the B.Sc., M.Sc., and Ph.D. degrees (summa cum laude) in ECE from The Ohio State University, Columbus, OH, USA, in 2005, 2007, and 2010, respectively.

He joined the Electrical Engineering Department, Petroleum Institute (PI), Abu Dhabi, United Arab Emirates, as an Assistant Professor, in 2010. He was promoted to Associate Professor in 2015. Since 2020, he has been a Professor with the Electrical Engineering Department, Khalifa University, Abu Dhabi, where he is currently an Associate Provost for Research. He has accomplished and has been working on several research projects at international and national levels (exceeding 25M USD). He is the Head of the Energy Systems, Control and Optimization Laboratory, ADRIC, and the Industry Engagement Theme Lead of the Advanced Power and Energy Center. He has one U.S. patent, one edited book, 12 book chapters, and over 280 scientific articles in top-tier journals and refereed international conference proceedings. He has supervised/cosupervised over 30 Ph.D./master students. His research interests include the applications of control and estimation theory on power systems stability, microgrids and smart grids, renewable energy systems and integration, and process control.

Dr. Al-Durra is an Editor of IEEE TRANSACTIONS ON SUSTAINABLE ENERGY and IEEE POWER ENGINEERING LETTERS and an Associate Editor of IEEE TRANSACTIONS ON INDUSTRY APPLICATIONS, *IET Renewable Power Generation*, and *IET Generation Transmission and Distribution*. In 2014, he obtained the PI Research and Scholarship Award for Junior Faculty, and he was elevated to the grade of IEEE Senior Member. He was awarded the United Arab Emirates Pioneers Award—United Arab Emirates Scientists in 2018. He was the Winner of the prestigious Khalifa Award for Education—Distinguished University Professor in Scientific Research from 2018 to 2019. He was awarded the Faculty Research Excellence Award-Khalifa University in 2020.

Ehab El-Saadany (Fellow, IEEE) was born in Cairo, Egypt, in 1964. He received the B.Sc. and M.Sc. degrees in electrical engineering from Ain Shams University, Cairo, in 1986 and 1990, respectively, and the Ph.D. degree in electrical engineering from the University of Waterloo, Waterloo, ON, Canada, in 1998.

He is currently an IEEE Fellow for his contributions to distributed generation planning, operation, and control. He was a Professor with the ECE Department, University of Waterloo, until 2019, where he was the Director of the Power M.Eng. Program from 2010 to 2015. He is currently a Professor with the Department of Electrical Engineering and the Dean of the College of Engineering and Physical Sciences, Khalifa University, Abu Dhabi, United Arab Emirates. He is an Internationally Recognized Expert in the area of sustainable energy integration and smart distribution systems. He is a Registered Professional Engineer in Ontario. His research interests include smart grid operation and control, microgrids, self-healing, cyber–physical security of smart grids, protection, power quality, embedded generation, and transportation electrification. He is a Registered Professional Engineer in Ontario.

Dr. El-Saadany was a two-time recipient of the Canada Research Chair Award in Energy Systems from 2009 to 2014 and Smart Distribution Systems from 2014 to 2018, the Mission Innovation Champion Award in 2020, the prestigious Khalifa Award in 2021, and the 2023 Mohamed Bin Rashid Medal for Scientific Excellence.